Nigerian Journal of Physics (NJP)
ISSN online: 3027-0936
ISSN print: 1595-0611
DOI: https://doi.org/10.62292/njp.v35i3.2026.518
Volume 35(3), September 2026

Enhancing the Visibility of Microcalcifications in Breast Tissue Using Morphological Operations and Gaussian Smoothing Techniques: A Phantom Study

***[1]Franca Oyiwoja Okoh, [2]Norlaili Ahmad Kabir, [1]John Actor Ocheje, [3]Mohd Fahmi Mohd Yusof, [4]Ahmad Sufril Azlan Mohammed, [5]Rafidah Zainon, [1]Onudibia Moses Ejike and [1]Yangde Ezekiel**

[1]Department of Pure and Applied Physics, Federal University Wukari, PMB 1020 Wukari-Taraba State, Nigeria
[2]School of Physics, Universiti Sains Malaysia, 11800 Penang, Malaysia
[3]School of Health Sciences, Universiti Sains Malaysia, 16150 Kelantan, Malaysia
[4]School of Computer Science, Universiti Sains Malaysia, 11800 Penang, Malaysia
[5]Advanced Medical and Dental Institute, Universiti Sains Malaysia, 13200 Penang, Malaysia

*Corresponding Author's Email: francaujah2005@yahoo.com

ABSTRACT

Breast cancer is one of the major causes of death among women. Microcalcification (MC) deposits could be an early sign of breast cancer. This study aims to investigate image contrast enhancement techniques that facilitate breast cancer diagnosis in dense breast tissues. A polyvinyl alcohol (PVAL) breast phantom, with embedded MCs was produced. Acquired mammogram images were analysed using morphological operations and the Gaussian smoothing techniques to enhance image contrast. The performances of all the filters were measured qualitatively by visual inspection, and quantitatively by evaluating the MSE, PSNR, and SNR. All experiments were conducted on MATLAB R2020a platform. Qualitative analysis showed that the Gaussian Smoothing filter recorded the best performance. Quantitatively, Low values of MSE with high PSNR/SNR depict better image quality enhancement. The closing morphological filter recorded the least mean value of MSE (32.86 ± 1.30) with the highest PSNR and SNR of 32.97 ± 0.20 and 22.91 ± 0.13 respectively. The Gaussian Smoothing filter came second with MSE, PSNR and SNR values equals 287.43 ± 10.65, 23.55 ± 0.17 and 12.83 ± 0.29 respectively. Therefore, the closing morphological filter produced a superior result quantitatively.

Keywords:
Breast cancer,
Microcalcification,
Morphological operations,
Gaussian Smoothing,
MSE,
SNR.

INTRODUCTION

Breast cancer is one of the major causes of fatality among women. MC deposits are the earliest suspicious signs of breast cancer. Breast density is one of the predisposing factors for breast cancer, and the risk of breast cancer is 4-6 times higher in women with dense breast tissue (Jalalian et al., 2013). The major challenge for radiologists in detecting MCs is due to their small size (0.1–1 mm, mean diameter ~ 0.3 mm) and low contrast (Vivona et al., 2014) this is associated with the density and thickness of the breast. The Breast Imaging Reporting and Data System (BIRADS) developed by the American College of Radiology (ACR) has classified breast density on mammography into 4 categories in terms of the amount of fibro glandular and adipose tissue present in the breast. Category 1 breast is almost entirely fat (< 25% fibro glandular tissue), category 2 contains scattered areas of fibro glandular tissue (25 – 50% fibrous tissue), category 3 breast is heterogeneously dense (50 - 75% fibro glandular tissue) and category 4 is extremely dense breast containing more than 75% fibro glandular tissue (Gweon et al., 2013). BIRADS 3 and 4 categories are the likely candidates for breast cancer and at the same time pose a challenge in diagnosis. In light of the foregoing, this study will focus on the use of a breast phantom that mimic BIRADS 3 category breast (Norlaili et al., 2021). Mammography have been proven to be a powerful and reliable tool in the early detection of breast cancer in women who have no symptoms or signs of the disease. Although, mammography has significant limitations with a sensitivity of 85–90% for breast cancer detection (Dromain et al., 2013), this imaging modality is still applicable in both routine breast screening and symptomatic diagnosis (Hendrick et al., 2010). Low contrast is one of the major challenges encountered by radiologists when interpreting mammogram images

especially for patients with dense breast tissues. This results from a small difference between the intensity values of a pixel with the neighbouring pixels and could lead to false negative diagnosis. The image quality of any mammogram is key in the diagnosis of breast cancer. Computer aided detection (CAD) necessitates the use of the computer to assist radiologists in breast cancer diagnosis. The use of CAD have demonstrated that more and smaller MCs can be detected, although at the expense of a slightly higher recall rate (Bick & Diekmann, 2007). CAD systems have greatly improved mammographic detection of breast cancer at screening by reducing the number of false-negative interpretations (Joseph et al., 2017; Kshema et al., 2017). Past studies have shown that digital image pre and post processing techniques were used to enhance mammogram image quality (Akila et al., 2015; Bandyopadhyay, 2010; Joseph et al., 2017; Lee et al., 2019; Ponraj & Jenifer, 2011). This study was carried out to assess the improvement in the visibility of MCs on mammograms of dense breast tissues by applying the morphological (erosion, dilation, opening and closing) and Smoothing filters.

MATERIALS AND METHODS

Phantom and image acquisition

The American College of Radiology (ACR) has classified breast density into 4 categories based on the amount of adipose versus fibroglandular tissue present. Based on characterization results from our previous study (Norlaili et al., 2021), 10 wt % PVAL solid gel with physical density of 1.056 ± 0.02 g/cm^3 was produced through freezing and thawing, to simulate a dense breast tissue (BIRADS category C). The MC material of choice was developed from a 50/50 blend of Calcium Carbonate and Graphite powder, resulting in small elements with a mass density of 2.21 g/cm^3. Each grouping of MC was made up of 6 granules with sizes defined by a range of values as shown in Table 1. The phantom was 4.5 cm thick; this is synonymous with the average compressed breast thickness. Figure 1 shows the fabricated phantom and mammogram image of phantom acquired using FFDM. The Image was acquired at the radiology department, Advanced Medical and Dental Institute (AMDI) Universiti Sains Malaysia (USM) on a Siemens Mammomat Revelation 1303, Germany at 28 kVp with automatic mAs setting.

Table 1: Dimensions associated with the micro calcifications (MCs)

MC	1	2	3	4	5
Size (µm)	>800	601-800	501-600	401-500	151-400

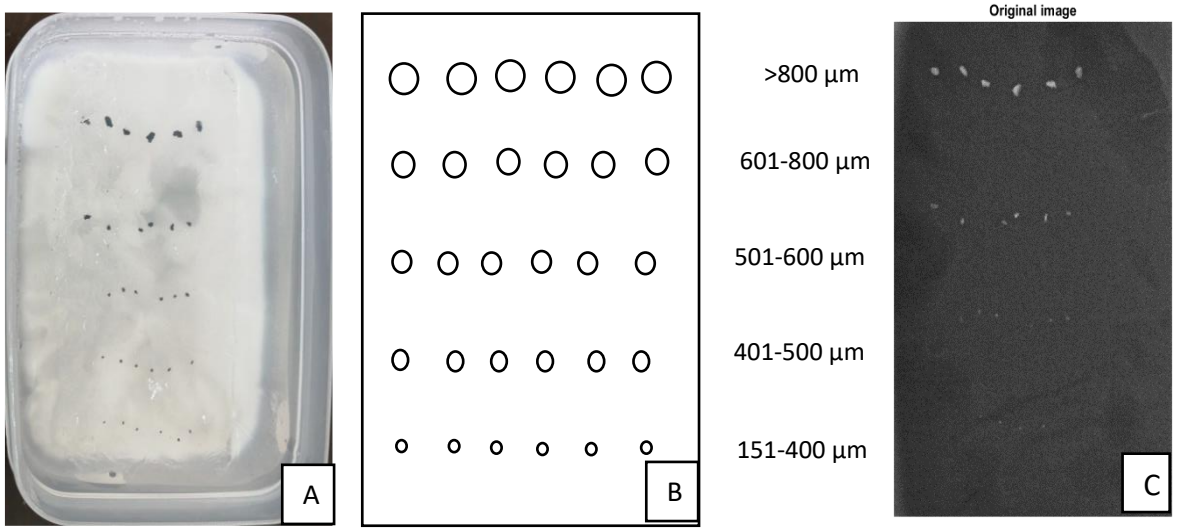

Figure 1: (a) Fabricated breast phantom with embedded microcalcification (b) schematic diagram of the breast phantom showing dimensions associated with microcalcification and (c) original mammogram image of phantom acquired from FFDM

Pre-processing

Noises are random fluctuations or variations in the brightness or colour information on an image which may be produced while capturing the image (Joseph et al., 2017). Digital mammograms are generally difficult to interpret as they are mostly characterized by some level of noise and low contrast between image background and lesions, hence, a preparatory phase is necessary to enhance the image quality and make the segmentation results more accurate. Pre-processing techniques are crucial in order to reduce noise, limit the search for abnormalities without undue influence from background of the mammogram (Bandyopadhyay, 2010; Ponraj & Jenifer, 2011). Two categories of pre-processing filters;

Morphological operations and Gaussian elimination were applied on the acquired mammogram to enhance the quality of the image. Considering the various sizes of MC employed, 5 equal regions of interests (ROI) were selected from the acquired phantom mammogram (Figure 1c) before the application of the various filters.

Morphological operations

Morphological operations such as dilation, erosion, opening, and closing can be applied through image filtering to grow or shrink image regions, as well as to remove or fill-in image region boundary pixels. The value of each pixel in the output image is based on a comparison of the corresponding pixel in the input image with its neighbours (Dubey et al., 2010). These fundamental operators process the input image based on the features encoded in the chosen structuring element. The morphological operations are applied on the grayscale mammography images to segment the abnormal regions (Ponraj & Jenifer, 2011).

Erosion and dilation

Erosion and dilation are the two basic operations in Mathematical Morphology (Gonzalez & Woods, 2002; Danladi et al., 2025). A combination of these two constitute the rest of the morphological operations. Erosion removes pixels on object boundaries whereas dilation adds pixels to the boundaries of objects in an image. The total number of pixels that are removed or added to the objects in an image is a function of the size and shape of the structuring element employed. Previous studies have demonstrated that small-sized disk structuring elements are well-suited for detecting and enhancing small, approximately circular features in medical images, as larger structuring elements may lead to over-smoothing and loss of diagnostically relevant information (Reljin et al., 2009; Gonzalez & Woods, 2018). Hence, in this work, we employed the 'disk' structuring element with radius of 2. The erosion of f by a non-flat (non-zero) structuring element b(s,t) is given by Equation 1.

$$[f \ominus b](x,y) = \min_{(s,t)\in b}\{f(x+s,y+t) - b(s,t)\} \quad (1)$$

The dilation of a non-flat structuring element is represented by Equation 2

$$[f \oplus b](x,y) = \max_{(s,t)\in b}\{f(x-s,y-t) + b(s,t)\} \quad (2)$$

Opening and closing

Erosion and dilation are combined to form other useful operators called opening and closing. Opening operation is obtained by doing dilation on eroded Image. This operator is used to remove small objects from an image and smooth the border of large objects. On the other hand, closing operation is achieved by doing erosion on a dilated image. closing removes small holes from an image. These techniques can also be used to find specific shapes in an image. The grey-scale mammographic images were separately filtered using open and close morphological operations. Equations 3 and 4 represents the mathematical expressions for the open and close operators, respectively.

Opening

$$f \circ b = (f \oplus b) \ominus b \quad (3)$$

Closing

$$f \bullet b = (f \ominus b) \oplus b \quad (4)$$

Gaussian Smoothing

The Gaussian smoothing operator is a 2-D convolution filter that is commonly used to `blur' an image thereby reducing detail and noise. This filter minimizes the low and high signals from distortion (Kshema et al., 2017). The degree of smoothing is controlled by the standard deviation (σ) of the Gaussian kernel, where larger σ values result in stronger blurring and smaller σ values retain more fine detail (Gonzalez & Woods, 2018). A moderate value of σ = 2 was selected in this study to achieve an optimal balance between noise suppression and edge preservation. The Gaussian elimination algorithm was based on the mathematical description in Equation 5.

$$G(x,y) = \frac{1}{2\pi\sigma^2} e^{-(x^2+y^2)/(2\sigma^2)} \quad (5)$$

Where x is the distance from the origin in the horizontal axis, y is the distance from the origin in the vertical axis and σ is the standard deviation of the Gaussian distribution.

Segmentation by adaptive thresholding

Image segmentation separates an image into multiple sections. The aim of this process is typically to enhance location of objects and boundaries. In image segmentation, the inputs are usually images while the outputs are the attributes extracted from those images. The extent to which image segmentation is implemented depends on the problem at hand. For the segmentation of intensity images like digital mammograms, one of the recommended approaches is the use of the thresholding technique (Ponraj & Jenifer, 2011). This technique assumes that all pixels whose gray level values falls within a given range belong to one class. This work employed the adaptive thresholding technique in separating the mammogram images into MCs and background.

$$g(x,y) = \begin{cases} 1 \; if \; f(x,y) > T \\ 0 \; if \; f(x,y) \le T \end{cases} \quad (6)$$

T is the Threshold that separates object from background. In adaptive thresholding, the value of T changes over an image as T depends on the spatial coordinates (x,y).

Proposed Algorithm

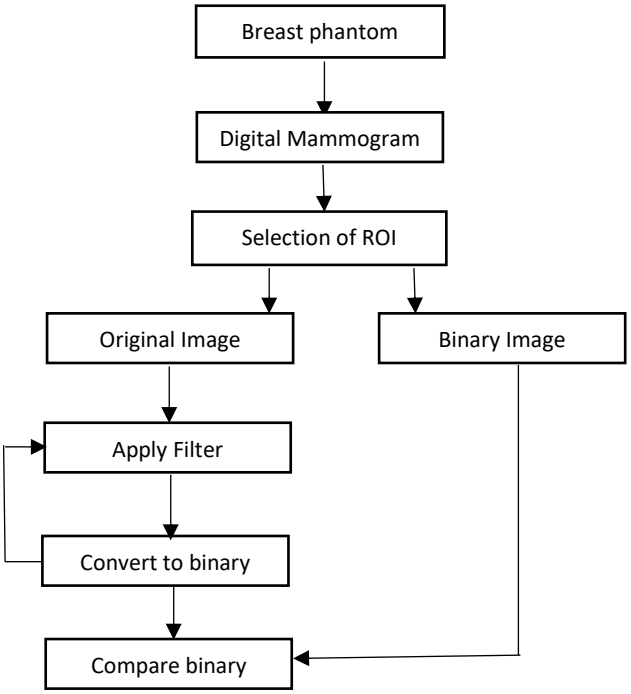

Figure 2: Proposed image processing flowchart

Measurement of filter performance

In the analysis of the performance of the various filters used, we calculated image quality metrics (IQM) such as the mean square error (MSE), peak signal to noise ratio (PSNR) and signal to noise ratio (SNR) for each image, these IQM are popular, simple and easy to evaluate (Isa et al., 2015; Zhang et al., 2012). MSE constitutes the cumulative squared error between the original (input) image and the resultant (output) image. Lower values of MSE signifies a low degree of error between the input and output image. The PSNR and SNR are very useful in demonstrating the visibility of an object. PSNR is defined as relative to peak dynamic range i.e. 255 for an 8 bit image (Isa et al., 2015). This parameter is used to quantify the image quality after reconstruction. A higher value of PSNR implies a good reconstruction and consequently, a higher image quality. The ratio of the mean signal power to the mean noise power defines the SNR. According to the Rose criterion, an object can be perceived and detected if the value of SNR ≥ 5 (Bushberg et al, 2011). Equation 7, 8 and 9 are the mathematical representations of MSE, PSNR and SNR respectively.

$$MSE = \frac{1}{M.N}\sum_{m=0}^{m=1}\sum_{n=0}^{n=1}\left[I(m,n) - \hat{I}(m,n)\right]^2 \quad (7)$$

Where I is the original image, $\hat{I}$ is the estimation of the original image obtained from a noisy image, M and N are the number of rows and columns in the input and output images correspondingly.

$$PSNR = 10log_{10}\frac{255^2}{MSE} \quad (8)$$

$$SNR = \frac{P_{signal}}{P_{noise}} \quad (9)$$

where P is average power.

RESULTS AND DISCUSSION

The experiments were conducted on MATLAB R2020a platform. Two analyses were applied for image pre-processing namely the qualitative and quantitative analysis. The qualitative analysis is based on visual inspection while quantitative analysis is achieved by evaluating the MSE, PSNR, and SNR. The results for both analyses are presented in Qualitative and Quantitative analysis sections.

Qualitative Analysis

Figure 3 presents grayscale and binary mammogram images of ROI 1 - 5 after undergoing image enhancement using erosion, dilation, opening, closing and Gaussian elimination. The grayscale and binary images of the original mammogram is represented by (a), while (b) – (f) represents the grayscale and binary images of the output after erosion, dilation, opening, closing and Gaussian smoothing respectively. By visual perception, the mammogram images that underwent morphological dilation and Gaussian smoothing depicted better enhancement among all the filtered images while erosion and closing caused the MCs to become constricted. The binary images were visually assessed based on the number of visible MCs on each ROI. Even though the number of visible MC may be the same for the original and enhanced binary images for a particular ROI, the MCs are more obvious in the processed binary images.

For example, 4 MCs appeared on the binary images of both the original and all the processed images of ROI 4 but the MCs are more obvious in (d) and (f) which were processed by opening and Gaussian smoothing filters respectively compared to the original binary image. It was not possible to distinguish MCs with diameter less than 400 μm (ROI 5) in any of the binary images except (f). The visual interpretation was supported by quantitative measurement; MSE, PSNR and SNR as demonstrated in the Quantitative Analysis section for each resultant image.

ROI 1

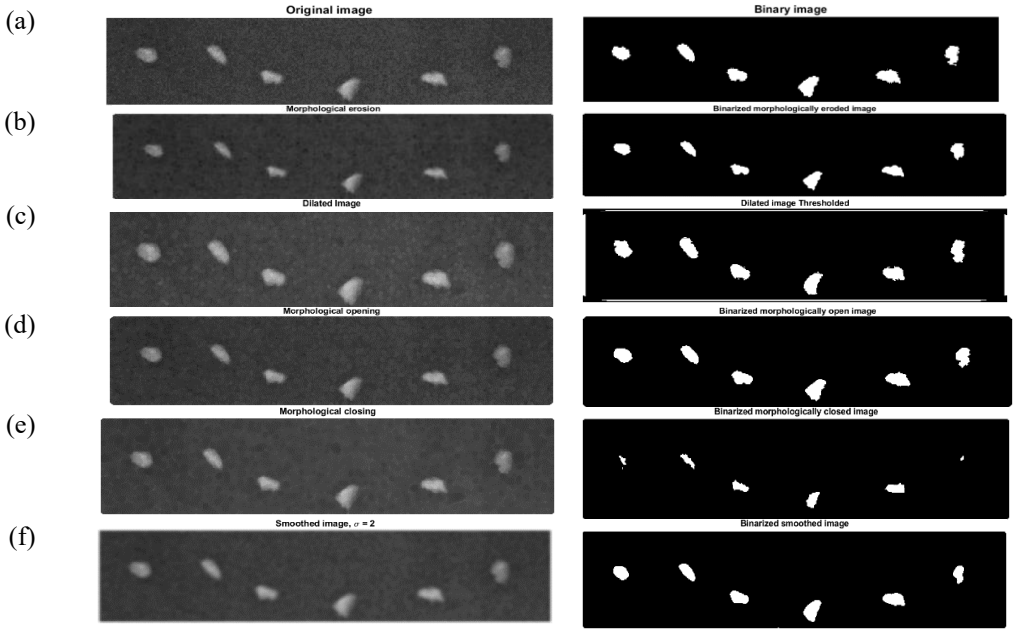

ROI 2

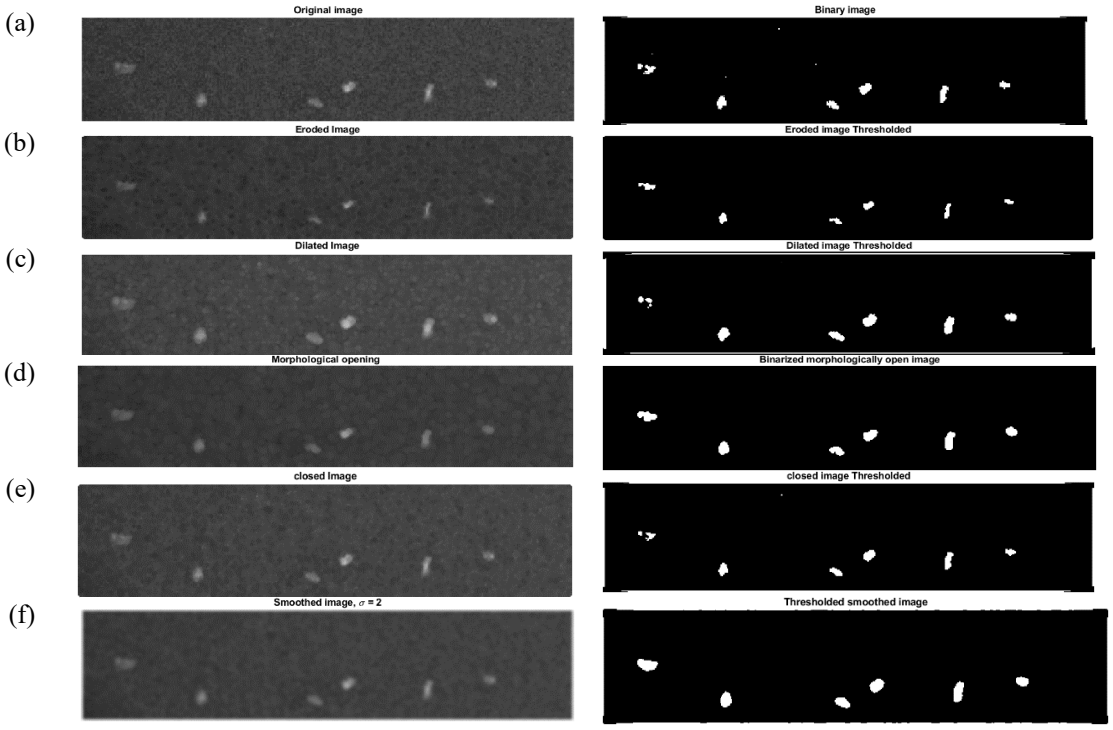

ROI 3

(a)

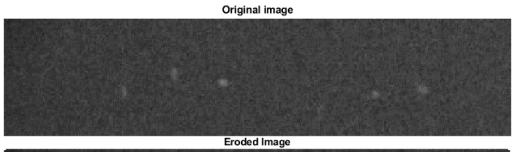

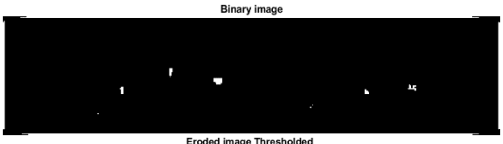

(b)

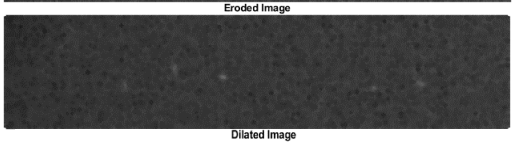

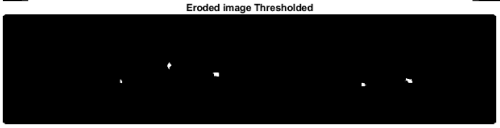

(c)

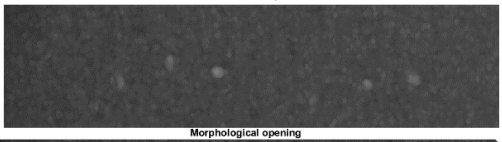

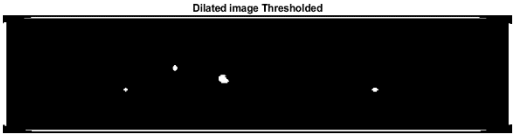

(d)

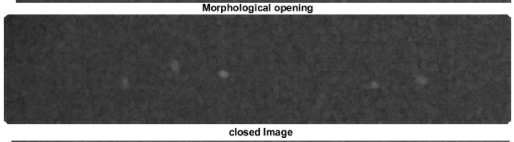

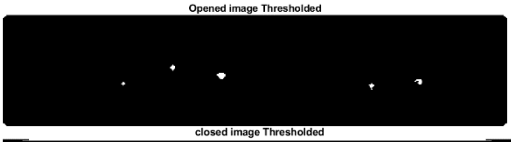

(e)

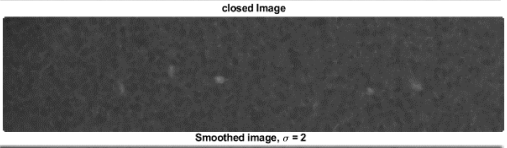

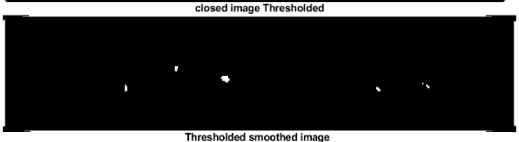

(f)

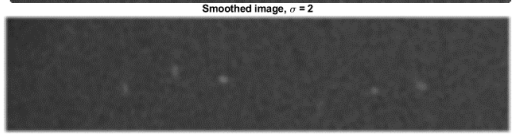

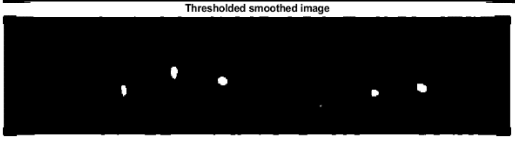

ROI 4

(a)

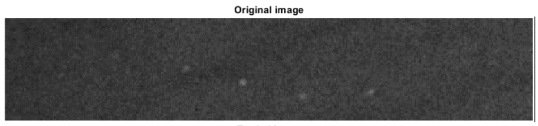

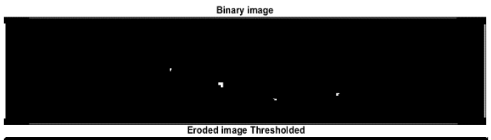

(b)

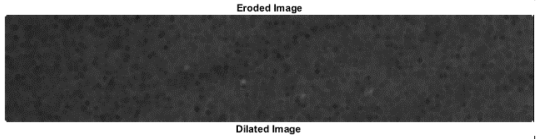

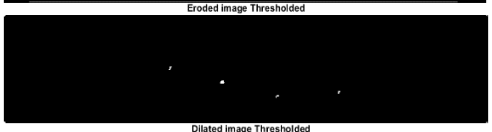

(c)

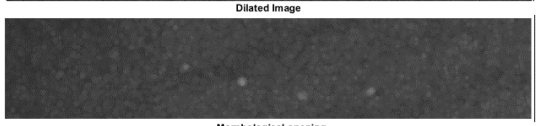

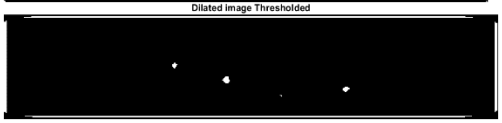

(d)

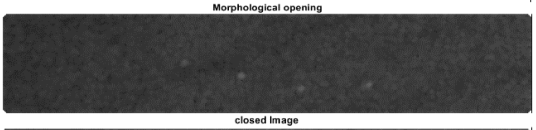

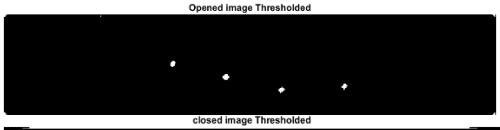

(e)

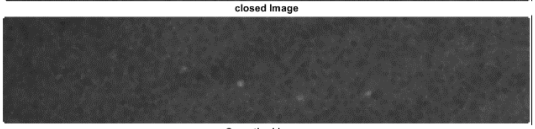

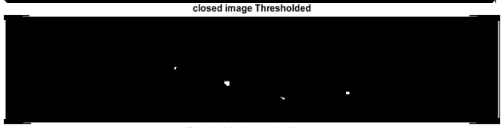

(f)

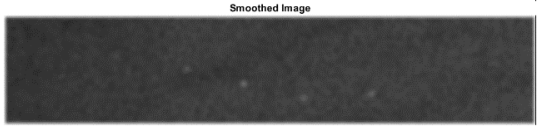

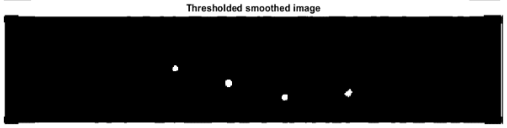

ROI 5

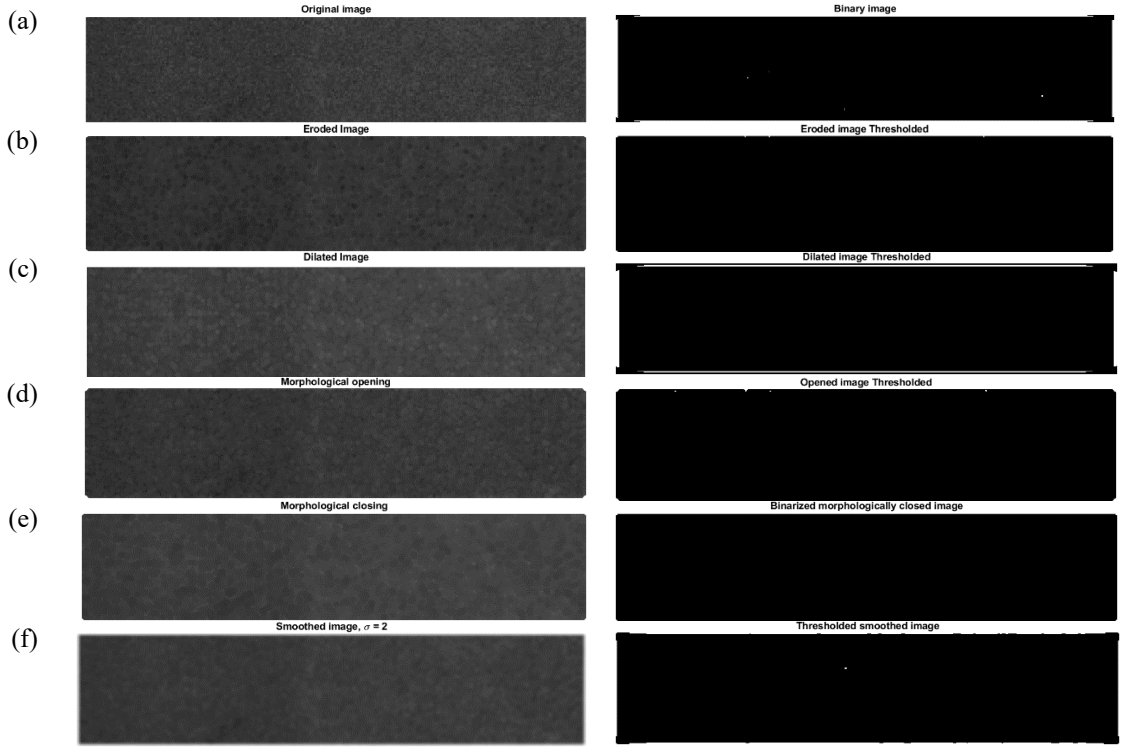

Figure 3: Grayscale and binary images of ROI 1 - 5 (a) Original (b) Eroded (c) Dilated (d) Opened (e) Closed (f) Gaussian Smoothing

Quantitative Analysis

Figure 4 shows the average MSE values of each tested filter namely erosion, dilation, opening, closing and Gaussian smoothing. The result revealed that the closing morphological operation yielded the least MSE followed by the Gaussian Smoothing filter compared to other filters. Higher values of MSE imply lower image quality. Figures 5 and 6 display the average PSNR and SNR values of each tested filter that was used to remove noise from the images. In comparing all 5 filters, the closing morphological operation and Gaussian Smoothing filter performed better compared to the other filters used.

The results of the analysis of variance (ANOVA) conducted across the five ROIs demonstrate an exceptionally high level of statistical similarity among the evaluated image quality metrics. Specifically, the ANOVA yielded P-value of 0.99 ($P > 0.05$) each for MSE, PSNR, and SNR. These values, being extremely close to unity, indicate that there are no statistically significant differences in the measured metrics for any particular image processing technique across the five ROIs. This shows that the ANOVA results strongly support the reliability and stability of the applied method, reinforcing its suitability for applications requiring homogeneous image quality across multiple regions of interest.

Overall, the use of Gaussian Smoothing technique depicted better image enhancement based on visual inspection even though it recorded the second-best result for quantitative analysis. The closing morphological operation recorded the least MSE and highest PSNR and SNR. It is seen that though there is not a single winner, Gaussian Smoothing and closing seem to have a superior performance compared to other filters used. This research revealed that, though the mammogram images visually showed better enhanced image, as illustrated in Figure 2, the PSNR values do not interpret similar results. For example, the image quality in Figure 2 (b); dilation show better edge preservation and less blurring compared to closing. However, in terms of PSNR and SNR, the closing operation yielded much higher values which translates to better quality. This is showing that qualitative and quantitative evaluation are dependent on each other to support the filtering technique.

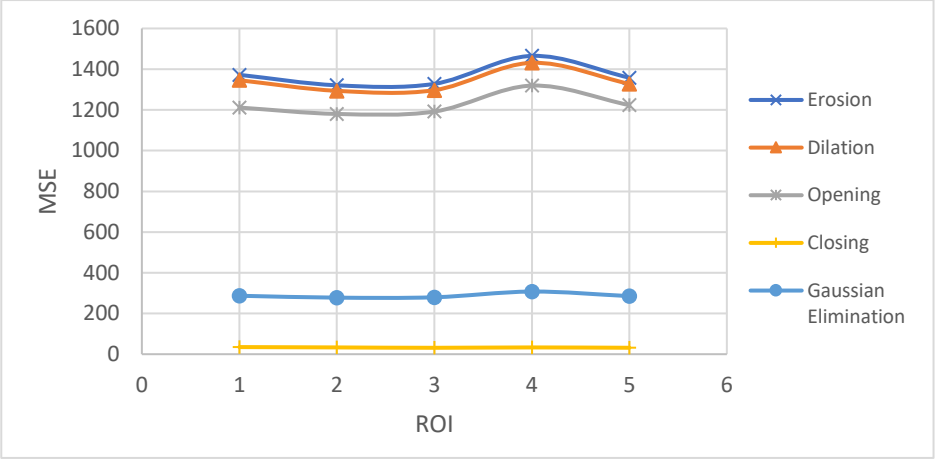

Figure 4: Performance of filter based on MSE

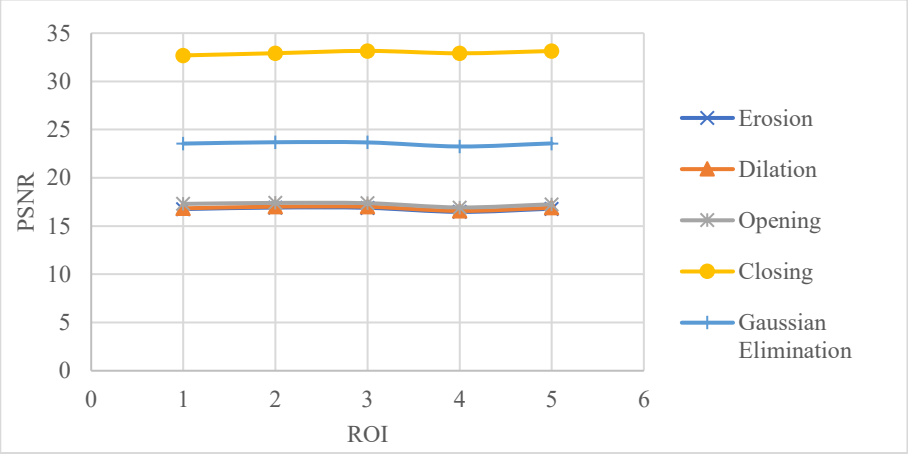

Figure 5: Performance of filter based on PSNR

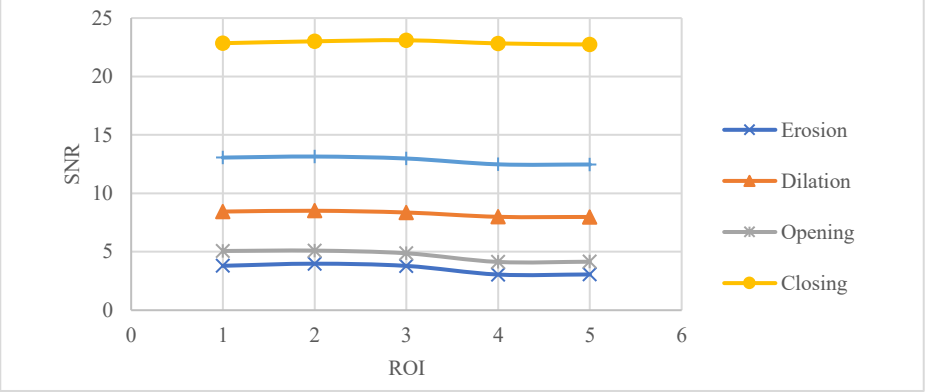

Figure 6: Performance of filter based on SNR

CONCLUSION

This paper assessed the impact of 4 mathematical morphological operations and the Gaussian smoothing algorithms on the improvement of the visibility of MCs on mammogram image. The main stages of image processing employed include ROI selection, pre-processing and segmentation of ROI. Morphological and Gaussian smoothing filters were used to enhance the image quality and segmentation of ROI was done by adaptive thresholding. Qualitative analysis via visual inspection identified Gaussian Smoothing as superior, while closing morphology performed best quantitatively; both outperformed erosion, dilation, and opening.

ACKNOWLEDGEMENT

The authors would like to acknowledge the financial support from Universiti Sains Malaysia (USM) under FRGS grant number FRGS/1/2018/STG02/USM/03/3/6711631 and the Radiology Department, Advanced Medical and Dental Institute (AMDI) USM.

REFERENCES

Akila, K., Jayashree, L. S., & Vasuki, A. (2015). Mammographic image enhancement using indirect contrast enhancement techniques - A comparative study. *Procedia Computer Science*, *47*(C), 255–261. https://doi.org/10.1016/j.procs.2015.03.205

Bandyopadhyay, S. K. (2010). Pre-processing of Mammogram Images. *International Journal of Engineering Science and Technology*, *2*(11), 6753–6758. https://www.researchgate.net/profile/Samir-Bandyopadhyay/publication/50384221_Pre-processing_of_Mammogram_Images/links/09e4150b8513bba519000000/Pre-processing-of-Mammogram-Images.pdf

Bick, U., & Diekmann, F. (2007). Digital mammography: What do we and what don't we know? *European Radiology*, *17*(8), 1931–1942. https://doi.org/10.1007/s00330-007-0586-1

Bushberg, Jerrold T., Seibert, J. Anthony, Leidholdt, Edwin M., & Boone, J. M. (2011). Signal-to-noise ratio. In C. W. Michell (Ed.), *The Essential Physics of Medical Imaging* (3rd ed., pp. 91–92). Wolter, Kluwer Lippincott, Williams & Wilkins.

Danladi, C., Mohammed, A. S. & Usman, A. (2025). A Computer Vision-Based Vehicle Speed Monitoring and Reporting System. *Nigerian Journal of Physics.* 34(3), 53-64. https://doi.org/10.62292/njp.v34i3.2025.382

Dromain, C., Boyer, B., Ferre, R., Canale, S., Delaloge, S., & Balleyguier, C. (2013). Computed-aided diagnosis (CAD) in the detection of breast cancer. *Eur J Radiol*, *82*(3), 417–423. https://doi.org/10.1016/j.ejrad.2012.03.005

Dubey, R. B., Hanmandlu, M., & Gupta, S. K. (2010). A comparison of two methods for the segmentation of masses in the digital mammograms. *Computerized Medical Imaging and Graphics*, *34*(3), 185–191. https://doi.org/10.1016/j.compmedimag.2009.09.002

Gonzalez, R. C., & Woods, R. E. (2018). *Digital Image Processing* (4th ed.). Pearson.

Gonzalez, R. C., & Woods, R. E. (2002). *Digital Image Processing* (second). Prentice-Hall.

Gweon, H. M., Youk, J. H., Kim, J. A., & Son, E. J. (2013). Radiologist assessment of breast density by BI-RADS categories versus fully automated volumetric assessment. *AJR Am J Roentgenol*, *201*(3), 692–697. https://doi.org/10.2214/AJR.12.10197

Hendrick, R. E., Pisano, E. D., Averbukh, A., Moran, C., Berns, E. A., Yaffe, M. J., Herman, B., Acharyya, S., & Gatsonis, C. (2010). Comparison of acquisition parameters and breast dose in digital mammography and screen-film mammography in the American College of Radiology Imaging Network digital mammographic imaging screening trial. *AJR Am J Roentgenol*, *194*(2), 362–369. https://doi.org/10.2214/AJR.08.2114

Isa, I. S., Sulaiman, S. N., Mustapha, M., & Darus, S. (2015). Evaluating denoising performances of fundamental filters for T2-weighted MRI images. *Procedia Computer Science*, *60*(1), 760–768. https://doi.org/10.1016/j.procs.2015.08.231

Jalalian, A., Mashohor, S. B., Mahmud, H. R., Saripan, M. I., Ramli, A. R., & Karasfi, B. (2013). Computer-aided detection/diagnosis of breast cancer in mammography and ultrasound: a review. *Clin Imaging*, *37*(3), 420–426. https://doi.org/10.1016/j.clinimag.2012.09.024

Joseph, A. M., John, M. G., & Dhas, A. S. (2017). Mammogram image denoising filters: A comparative study. *2017 Conference on Emerging Devices and Smart Systems, ICEDSS 2017*, *March*, 184–189. https://doi.org/10.1109/ICEDSS.2017.8073679

Kshema, George, M. J., & Dhas, D. A. S. (2017). Preprocessing filters for mammogram images: A review. *2017 Conference on Emerging Devices and Smart Systems, ICEDSS 2017*, *August 2018*, 1–7. https://doi.org/10.1109/ICEDSS.2017.8073694

Lee, S., Jin Park, S., Jeon, J. M., Lee, M. H., Ryu, D. Y., Lee, E., Kang, S. H., & Lee, Y. (2019). Noise removal in medical mammography images using fast non-local means denoising algorithm for early breast cancer detection: a phantom study. *Optik*, *180*(November 2018), 569–575. https://doi.org/10.1016/j.ijleo.2018.11.167

Norlaili, A. K., Okoh, O. F., & Mohd Yusof, M. F. (2021). Radiological and Physical Properties of Tissue Equivalent Mammography Phantom: Characterization and Analysis Methods. *Radiation Physics and Chemistry*, https://doi.org/10.1016/j.radphyschem.2020.109271.

Ponraj, D., & Jenifer, M. (2011). A Survey on the Preprocessing Techniques of Mammogram for the Detection of Breast Cancer. *Journal of Emerging …*, *2*(12), 656–664.

Reljin, B., Miloševiæ, Z., Stojiæ, T and Reljin, I (2009). Computer aided system for segmentation and visualization of microcalcifications in digital mammograms. *Folia Histochem Cytobiol.* 47(3), 525-532

Vivona, L., Cascio, D., Fauci, F., & Raso, G. (2014). Fuzzy technique for microcalcifications clustering in digital mammograms. *BMC Medical Imaging*, *14*(1), 1–18. https://doi.org/10.1186/1471-2342-14-23

Zhang, Y., Cheng, H. D., Huang, J., & Tang, X. (2012). An effective and objective criterion for evaluating the performance of denoising filters. *Pattern Recognition*, *45*(7), 2743–2757. https://doi.org/10.1016/j.patcog.2012.01.015